



# Modeling of Stress Relaxation Modulus for a Nanocomposite Biosensor by Relaxation Time, Yield Stress, and Zero Complex Viscosity

YASSER ZARE <sup>1</sup> and KYONG YOP RHEE<sup>2,3</sup>

1.—Biomaterials and Tissue Engineering Research Group, Department of Interdisciplinary Technologies, Breast Cancer Research Center, Motamed Cancer Institute, ACECR, Tehran, Iran.  
2.—Department of Mechanical Engineering (BK21 four), College of Engineering, Kyung Hee University, 1 Seocheon, Giheung, Yongin, Gyeonggi 449-701, Republic of Korea.  
3.—e-mail: rheeky@khu.ac.kr

This paper presents a simple equation for the stress relaxation modulus,  $G(t)$ , of nanocomposite biosensor and blend films by relaxation time, yield stress, zero complex viscosity, and power-law index. The correctness of the advanced model is assessed by the measured results for the examples containing poly (ethylene oxide) (PEO), poly (lactic acid) (PLA) and carbon nanotubes. Furthermore, the roles of whole factors in  $G(t)$  are justified to approve the predictability of the advanced model. The model's predictions correctly fit the experimental facts and whole factors reveal acceptable trends. All parameters including yield stress, relaxation time, zero complex viscosity, power-law index, and the width of the transition section directly affect  $G(t)$ . The sensible results validate the advanced model, providing a simple procedure for approximating and optimizing  $G(t)$  in blend and nanocomposite systems.

## INTRODUCTION

Poly (lactic acid) (PLA) as a biocompatible and biodegradable polymer demonstrates the outstanding potential for replacement of oil-based polymers.<sup>1–5</sup> Moreover, PLA shows desirable biodegradability, nontoxicity, and high mechanical performance.<sup>6–8</sup> These attractive properties have stimulated studies on the properties and potential applications of PLA. However, some limitations, such as low toughness and slow degradation rate of PLA have restricted its development and application. Earlier studies have suggested many techniques to overcome these problems by mixing, plasticization, copolymerization, and fortification by filler.<sup>2,9–12</sup> It seems that the utilization of another polymer or nanoparticles is a beneficial and suitable way to control the degradation rate and improve the mechanical properties of PLA.<sup>13,14</sup>

Carbon nanotubes (CNT) are a superlative nanofiller for yielding high-grade nanocomposites. The high flexibility, small density, and great aspect ratio (relation of length to diameter) along with the excellent electrical, mechanical, and thermal performance of CNT have attracted researchers to CNT-based nanocomposites.<sup>15–22</sup> The large number of papers in this field confirms this statement. The electrical and mechanical performance of CNT-reinforced nanocomposites principally correlates to percolation onset and network size influenced by CNT size and interphase depth around CNT.<sup>23–26</sup>

The viscoelastic properties of polymer nanocomposites obtained by rheology can elucidate the nanostructure of nanoparticles.<sup>27,28</sup> So, rheological behavior is a powerful tool for investigation of morphology, because the viscoelastic characteristics are mostly sensitive to chain mobility and diffusion as well as interfacial interactions.<sup>29,30</sup> Generally, nanoparticle microstructure, polymer limitation by nanoparticles, or chemical or physical bonds to the solid surfaces of particles cause solid behavior in nanocomposites at the frequency sweep test, which restricts chain flexibility and lengthens the

relaxation time.<sup>31,32</sup> Since network breakdown in nanocomposites quickens the shear thinning performance in frequency tests,<sup>33,34</sup> it is acceptable to use rheological measurements to examine the extent of networks in nanocomposites. From a theoretical point of view, few models can examine the loss modulus, storage modulus, complex viscosity, and complex modulus in polymer nanocomposites.<sup>35–38</sup> The earlier reports mainly applied these models to analyze rheological measurements.<sup>39,40</sup> They commonly calculated some parameters such as relaxation time, power-law index, and zero complex viscosity by comparing the experimental results with the predictions. However, the models expressing the stress relaxation modulus [ $G(t)$ ] for polymer systems are extremely limited.

Schwarzl<sup>41</sup> suggested a numerical formula for the variation of  $G(t)$  with time by storage and loss moduli. Tayefi et al.<sup>40</sup> have applied this equation to estimate the  $G(t)$  for nanocomposites containing uncured and cured ethylene-octene copolymer and organoclay. The present study aims to develop this equation by formulation of storage and loss moduli using Casson<sup>42</sup> and Carreau-Yasuda<sup>36</sup> models. Both storage and loss moduli are correlated to relaxation time, yield stress, zero complex viscosity, and power-law characteristics to extract a model for  $G(t)$ . Moreover, the storage and loss moduli of the specimens encompassing PEO, PLA, and CNT are measured at dissimilar frequencies. The model's predictions for  $G(t)$  are associated with the measured facts to approve the model and to calculate the parameters. Additionally, the influences of different factors on  $G(t)$  are justified to approve the model's estimations. The current model provides a simple approach, which can guide the authors when adjusting the  $G(t)$  and viscoelastic terms in various polymer systems.

## EQUATIONS

Schwarzl<sup>41</sup> proposed a numerical equation for  $G(t)$  by storage ( $G'$ ) and loss ( $G''$ ) moduli as well as frequency ( $w$ ) by:

$$G(t) \cong G'(w) - 0.56G''(w/2) + 0.2G''(w) \quad (1)$$

However, the higher levels of  $G''$  compared with  $G'$  produce negative  $G(t)$ , which is not acceptable. Therefore, we properly develop and simplify this model by numerical analyses as:

$$G(t) \cong G'(w) + 0.5G''(w) \quad (2)$$

This model can present the experimental results of  $G(t)$  by the experimental extents of moduli.

Now,  $G''$  and  $G'$  are formulated to express  $G(t)$  as a function of the viscoelastic parameter.

Bae et al.<sup>43</sup> suggested an equation for relaxation time ( $\lambda$ ) of polymer chains in nanocomposites by:

$$\lambda = \frac{G'}{|\eta^*|w^2} \quad (3)$$

where  $\eta^*$  is complex viscosity. This model can be reorganized to propose the storage modulus as:

$$G' = \lambda|\eta^*|w^2 \quad (4)$$

which correlates the  $G'$  to relaxation time and complex viscosity. Many models have been suggested for complex viscosity in nanocomposites,<sup>38</sup> but the best known model is Carreau-Yasuda,<sup>36</sup> which is defined as:

$$\eta^* = \eta_0^*[1 + (\lambda w)^a]^{\frac{n-1}{a}} \quad (5)$$

where  $\eta_0^*$  shows zero complex viscosity,  $n$  is the power-law index and  $a$  denotes the breadth of the Newtonian–power-law transition section.  $\eta_0^*$  is the complex viscosity at extremely low frequencies ( $w \approx 0$ ). This equation has been used in many studies to simulate complex viscosity.<sup>29,38</sup>

When  $\eta^*$  is substituted from the last equation into Eq. (2),  $G'$  is suggested as:

$$G' = \lambda\eta_0^*[1 + (\lambda w)^a]^{\frac{n-1}{a}}w^2 \quad (6)$$

expressing the storage modulus by various viscoelastic parameters.

Additionally, the loss modulus of a heterogeneous system was given based on the Casson model<sup>42</sup> as:

$$G''^{1/2} = \tau^{1/2} + Kw^{1/2} \quad (7)$$

where  $\tau$  is yield stress and  $K$  is a constant. This model was applied in previous articles to calculate the yield stress and  $K$ .<sup>31,43</sup> Using the Bingham model,<sup>44</sup> the flow happens in nanocomposites above yield stress, because the physical nets in nanocomposites inhibit the melt flow.<sup>45</sup>

The reorganization of the latter equation results in:

$$G'' = (\tau^{1/2} + Kw^{1/2})^2 \quad (8)$$

When  $G'$  [Eq. (6)] and  $G''$  [Eq. (8)] are substituted into Eq. (2),  $G(t)$  is specified by:

$$G(t) \cong \lambda\eta_0^*[1 + (\lambda w)^a]^{\frac{n-1}{a}}w^2 + 0.5(\tau^{1/2} + Kw^{1/2})^2 \quad (9)$$

which represents  $G(t)$  as a function of many parameters such as relaxation time, zero complex viscosity, yield stress, and power-law index. Undoubtedly, the strong interactions at the nanofiller-polymer interface produce the interphase section in the samples, which affects the nanocomposite's performance.<sup>46–49</sup> The interphase section influences the  $\eta_0^*$ ,  $\tau$ , and  $K$ , as expected. Actually, the interphase characteristics affect the mentioned parameters, but the interfacial/interphase section in the samples cannot affect the predictability of the developed model.

## EXPERIMENTAL PART

### Materials

Biopolymers PLA (ME346310) and PEO ( $M_v = 200,000$  g/mol) were delivered from Sigma-Aldrich. Also, Hanhwa Nanotech Co., Korea, provided the multi-walled CNT (MWCNT) (CM-95 grade) and Shindo Co., Korea supplied chloroform as the solvent for solution mixing.

### Preparation of Films

All films were made by solution processing in chloroform. The details for this technique are mentioned in Ref. 50. There is no residual solvent in the prepared films, because the films were dried at 45 °C under vacuum for 12 h. The samples are named PLA $x$ /PEO $y$ /CnT $z$  in which  $x$ ,  $y$ , and  $z$  present the weight portion of PLA, PEO, and CNT, in that order.

### Characterization

A Paar-Physica rheometer, with disk-type parallel plates with a diameter of 25 mm and 1-mm gap measured the dynamic rheological properties under a constant nitrogen atmosphere. The isothermal dynamic frequency sweep test was conducted at 1% strain and 180 °C from 0.01 to 628 rad/s. The morphology of samples was investigated on gold-coated samples using scanning electron microscopy (SEM) (XL30S) at an accelerating voltage of 10 kV.

## RESULTS AND DISCUSSION

### Morphology of Films

Figure 1 depicts the morphological images of nanocomposite films containing 1 wt% CNT. Figure 1a shows that the addition of 1 wt% CNT to the PLA60/PEO40 blend causes PEO islands in the PLA matrix, which can be seen as a matrix-droplet morphology. This image shows the uniform dispersion of small PEO particles in the PLA phase. Moreover, the light strips display the well-dispersed CNT in the film without aggregation/agglomeration, representing the strong interfacial interaction between polymer matrix and CNT. Figure 1b exhibits the morphology of the PLA75/PEO25/CNT1 sample demonstrating the PEO particles in the PLA phase. The dispersion of CNT in the PLA phase is homogeneous and CNT size does not exceed 100 nm, confirming the formation of nanostructure. Figure 1c shows the morphology of the PLA90/PEO10/CNT1 sample in which the separated PEO islands in the continuous PLA matrix are evident. It can be said that CNT encourages the blend to disperse the PEO particles in the PLA matrix. Also, the fine dispersion of CNT as light strips is distinct in the PLA without aggregation/agglomeration.

### Comparison Between Experimental and Theoretical Data

The experimentally measured storage and loss moduli are inserted into Eq. (2) to estimate the

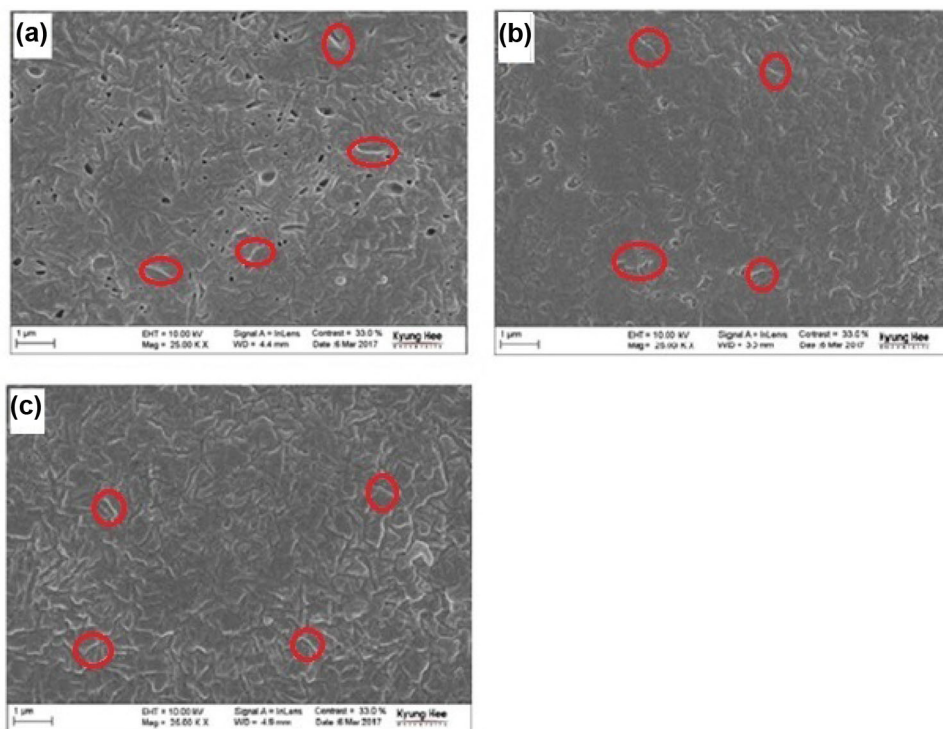


Fig. 1. SEM images of (a) PLA60/PEO40/CNT1, (b) PLA75/PEO25/CNT1, and (c) PLA90/PEO10/CNT1 samples. The labeled zones signify the CNT.

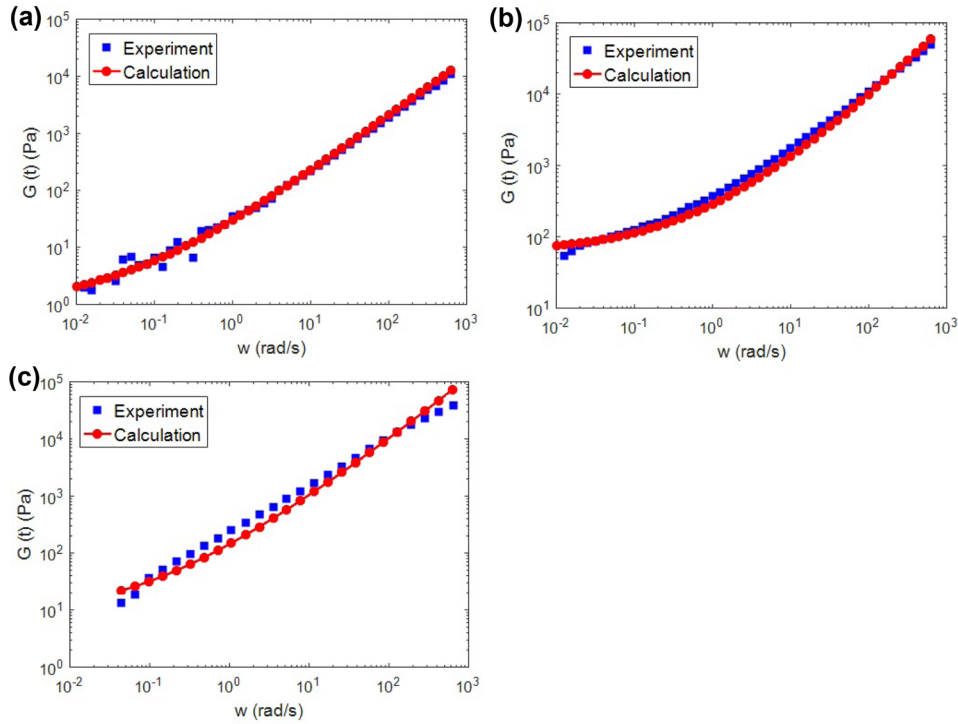


Fig. 2. Measured and calculated data for  $G(t)$  at different frequencies for (a) PLA60/PEO40, (b) PLA60/PEO40/CNT1, and (c) PLA60/PEO40/CNT2 samples.

**Table I. The model's calculations for the examples**

Samples	$\tau$ (Pa)	$K$ (Pa.s) <sup>1/2</sup>	$\eta_0^*$ (Pa.s)	$\lambda$ (s)	$n$	$\alpha$
PLA60/PEO40	3	6	100	0.001	0.25	0.03
PLA60/PEO40/CNT1	120	13	1000	0.007	0.15	0.01
PLA60/PEO40/CNT2	15	13	25000	0.020	0.05	0.01
PLA75/PEO25	2	7	1000	0.002	0.25	0.20
PLA75/PEO25/CNT1	50	25	25000	0.040	0.15	0.05
PLA75/PEO25/CNT2	37000	18	95000	0.100	0.04	0.01
PLA90/PEO10	0.5	8	100	0.002	0.35	0.25
PLA90/PEO10/CNT1	2000	35	15000	0.100	0.23	0.02
PLA90/PEO10/CNT2	9000	50	100000	0.200	0.10	0.01

experimental levels of  $G(t)$ . In addition, Eq. (9) can offer the calculation of  $G(t)$  as a function of frequency. The empirical quantities and the forecasts of  $G(t)$  were compared to test the established model.

Figure 2 illustrates the investigational data and the calculations of  $G(t)$  for the examples comprising 60 wt% PLA. The  $G(t)$  increases as frequency rises and thus a high frequency improves the  $G(t)$ . This trend is reasonable because the polymer chains resist short-range deformation (high frequency), while they easily relax at a long time period (low frequency). Moreover, the model's outputs follow the investigational data for all examples. This acceptable agreement confirms the model's predictability for  $G(t)$  as a function of the main parameters. The model's factors are presented in Table I. The PLA60/PEO40 sample demonstrates a poor yield stress, but

the nanocomposites exhibit high yield stress, because of the CNT physical nets. Also, the  $K$  constant increases when CNT is added to this blend.

The zero complex viscosity increases when CNT is added, because the nanoparticles and the interconnections between them mainly enhance the zero complex viscosity. In addition, the relaxation time enhances in nanocomposites, because the nanoparticles inhibit polymer movement.  $n$  also decreases in nanocomposites because the nanofiller strengthens the shear thinning of polymers. Also, the breadth of the transition section is narrower in nanocomposites, demonstrating that the nanofiller shortens the transition region and promotes power-law behavior. These reasonable calculations validate the developed model for  $G(t)$  in polymer systems.

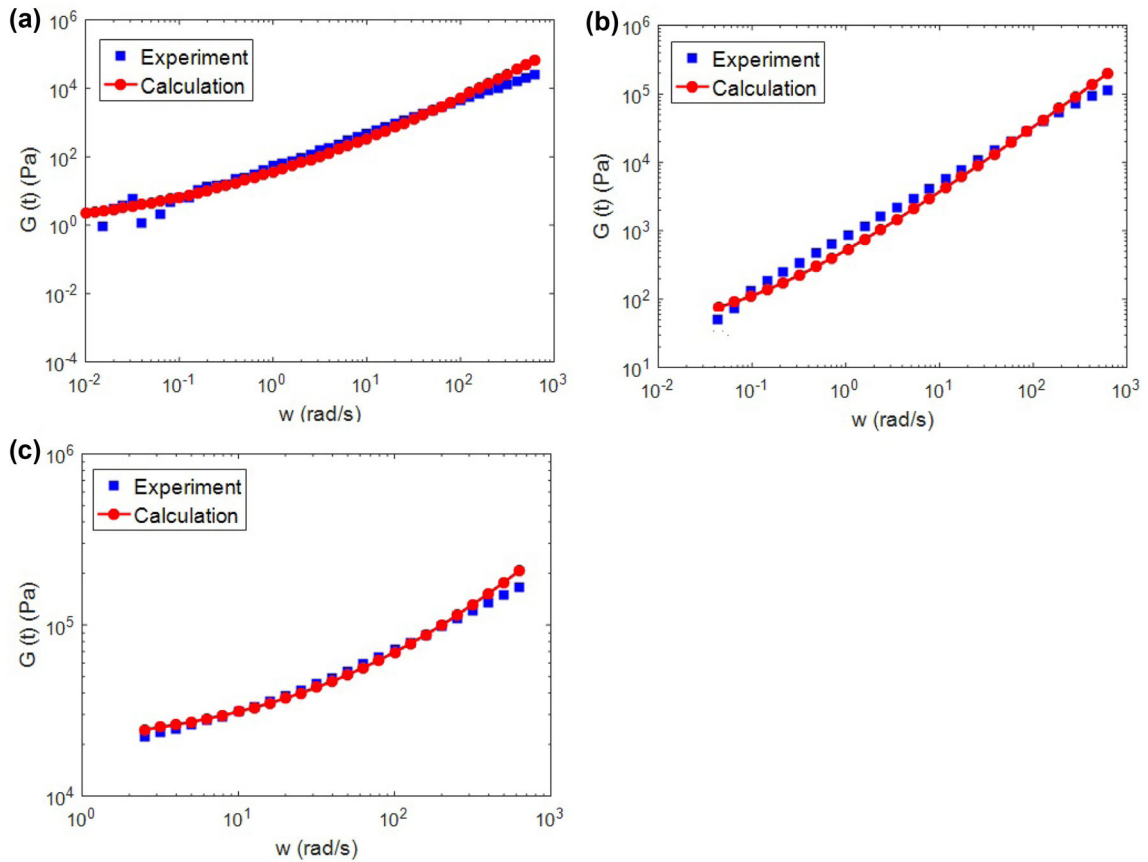


Fig. 3. Experimental and theoretical levels of  $G(t)$  at different frequencies for (a) PLA75/PEO25, (b) PLA75/PEO25/CNT1, and (c) PLA75/PEO25/CNT2 specimens.

Figure 3 represents the empirical and hypothetical levels of  $G(t)$  for the samples at 75 wt% PLA as a function of frequency. A high frequency increases the  $G(t)$  and the  $G(t)$  in nanocomposites is higher than that of polymer blends. This is due to the interactions among polymer chains and nanofiller restricting the relaxation. Furthermore, the calculations acceptably follow the experimental data in the samples at different frequency series. Hence, the advanced model properly predicts the  $G(t)$  in the blends and nanocomposites.

The parameters' calculations for the current examples are shown in Table I. The yield stress increases as expected in the nanocomposites, because CNT establish continuous nets in the samples, promoting yield stress. In addition,  $K$  changes in the blends and nanocomposites. Nevertheless, the incorporation of particles to the blend raises the zero complex viscosity, since the nets of CNT raise the solidity of nanocomposites at small frequencies. The relaxation time in nanocomposites is higher than in the polymer blend, owing to the polymer–nanoparticle connections, restricting chain movement. Moreover, the values of  $n$  and  $\alpha$  reduce in the nanocomposites, because the CNT strengthens the power-law performance and shortens the

transition section. All results are meaningful, and validate the developed models for  $G(t)$ .

Figure 4 displays the empirical and hypothetical data for  $G(t)$  for the industrialized models for the examples with 90 wt% PLA.  $G(t)$  expectedly progresses by frequency, since the polymer molecules do not have sufficient time for relaxation at high frequencies presenting high  $G(t)$ , while the simple relaxation of chains at low frequency (extensive time) produces a poor  $G(t)$ .

The  $G(t)$  in the nanocomposites is more than that of polymer blends, due to the positive role of nanoparticles in the stiffness of nanocomposites. The calculations of  $G(t)$  successfully fit to the experimental measurements indicating that the developed model acceptably predicts the  $G(t)$  in polymer products. Actually, the developed model properly estimates the  $G(t)$  assuming the yield stress, zero complex viscosity,  $K$ , relaxation time, and power-law parameters. Table I represents the values of terms for the cited examples. The incorporation of CNT in the blend enhances the yield stress, owing to the CNT net, which enhances the required stress for flowing. Additionally,  $K$  changes from 8 to 50 (Pa.s)<sup>1/2</sup> for the prepared samples, demonstrating the positive role of CNT in  $K$ . The zero complex viscosity also increases in the

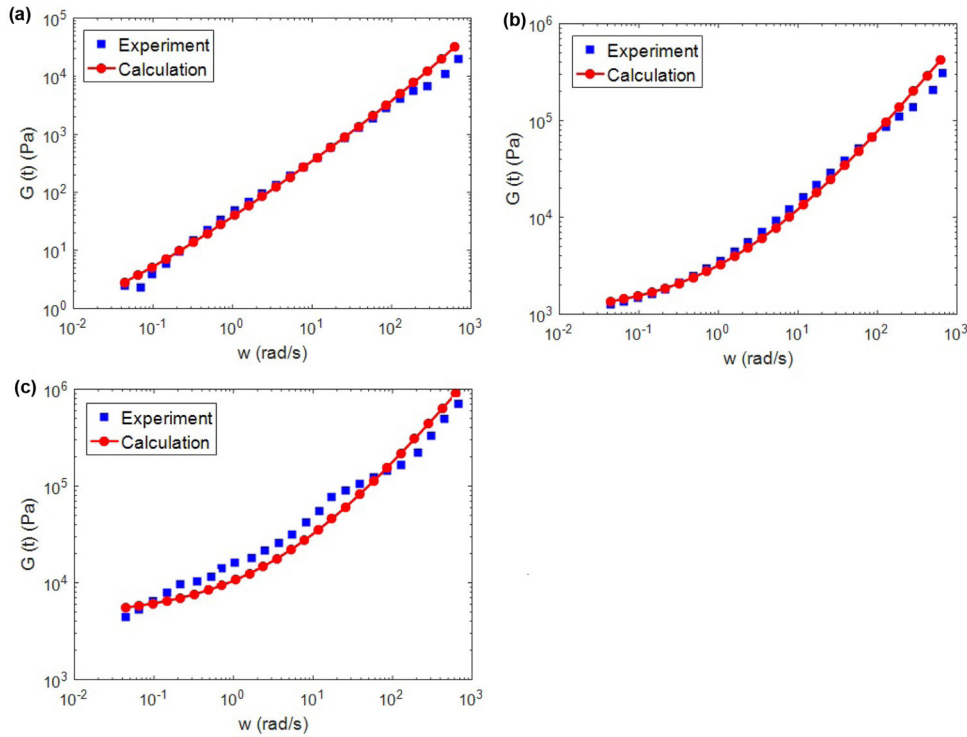


Fig. 4. Variation of  $G(t)$  data at different frequencies for (a) PLA90/PEO10, (b) PLA90/PEO10/CNT1, and (c) PLA90/PEO10/CNT2 specimens.

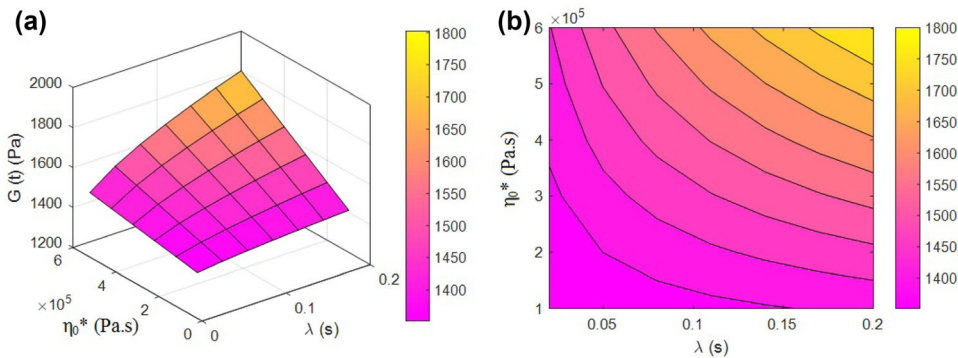


Fig. 5.  $G(t)$  dependence on relaxation time and zero complex viscosity by Eq. (9): (a) 3D and (b) contour patterns.

nanocomposites, since CNT nets establish a solid-form performance at low frequencies.<sup>51,52</sup> Furthermore, the nanoparticles lengthen the relaxation time, because they limit the polymer's flexibility. Also,  $n$  and  $a$  parameters reduce in nanocomposites, because the nanoparticles tend to strengthen and quicken the power-law behavior in nanocomposites. These results are expected, confirming the developed model for  $G(t)$ .

### Analysis of Parameters

All parameters' impacts on  $G(t)$  were examined to confirm the advanced model [Eq. (9)]. Undoubtedly, the reasonable effects of whole factors on  $G(t)$  authenticate the current model and guide the optimization of  $G(t)$ . 3D and contour designs show

the impacts of two variables on  $G(t)$  at normal values of other factors. In this study, the middling values of terms are  $K = 20 \text{ (Pa.s)}^{1/2}$ ,  $\omega = 1 \text{ rad/s}$ ,  $\tau = 1000 \text{ Pa}$ ,  $\eta_0^* = 300,000 \text{ Pa.s}$ ,  $\lambda = 0.1 \text{ s}$ ,  $n = 0.1$  and  $a = 0.1$ .

Figure 5 exhibits the correlation of  $G(t)$  to relaxation time and zero complex viscosity based on Eq. (9). The maximum values of  $\lambda = 0.2 \text{ s}$  and  $\eta_0^* = 6 \times 10^5 \text{ Pa.s}$  result in a  $G(t)$  of 1800 Pa, while  $\lambda < 0.05 \text{ s}$  and  $\eta_0^* < 2 \times 10^5 \text{ Pa.s}$  diminish  $G(t)$  to 1350 Pa. Accordingly, both relaxation time and zero complex viscosity directly affect  $G(t)$ . The high values of relaxation time and zero complex viscosity increase  $G(t)$ , while a short relaxation time and a minor zero complex viscosity produce a low  $G(t)$ .

A long relaxation time reveals the difficult relaxation of polymer molecules under packing. Accordingly, a long relaxation time limits polymer distortion during the test, which induces a big  $G(t)$ . Actually, a big relaxation time reduces the polymer tendency for distortion, which raises the  $G(t)$ . On the other hand, a small relaxation time introduces the simple relaxation and deformation of polymer molecules during the test, creating a poor  $G(t)$ . Therefore, the advanced model correctly demonstrates the relaxation time role in  $G(t)$ . In addition, a high zero complex viscosity is indicative of the large networks of CNT in the sample. In fact, the big networks cause a solid-form performance at small frequencies, which produces a high zero complex viscosity. Since the CNT nets confine the polymer's relaxation and stand against stress, the zero complex viscosity affects the  $G(t)$  in a desirable way. However, a low zero complex viscosity reveals the deprived networks in the sample, which cannot improve the  $G(t)$ , because they insignificantly manipulate the relaxation of polymer chains. Therefore, the zero complex viscosity positively governs  $G(t)$ , as shown by the advanced model.

Figure 6 depicts the effects of yield stress and  $K$  on  $G(t)$  using the developed model. The highest  $G(t)$  of 3500 Pa is obtained by  $\tau = 2000$  Pa and  $K = 40$  (Pa.s)<sup>1/2</sup>, while the  $G(t)$  mainly deteriorates to 650 Pa at  $\tau < 700$  Pa and  $K < 15$  (Pa.s)<sup>1/2</sup>. Thus, the yield stress and  $K$  parameter directly manipulate

$G(t)$ . Actually, the high levels of yield stress and  $K$  are necessary to raise the  $G(t)$  in nanocomposites. In contrast, the lower values of both yield stress and  $K$  meaningfully weaken the  $G(t)$ .

An extraordinary yield stress reveals how robust the CNT nets are in nanocomposites,<sup>45</sup> which develop the  $G(t)$ , because the big networks limit the relaxation of polymer chains. Conversely, a lower yield stress shows the formation of insignificant networks in the sample, which facilitates the relaxation of polymer chains and worsens the  $G(t)$ . Moreover, a high  $K$  enhances the loss modulus based on Eq. (8). Indeed, a big  $K$  increases the modulus of viscous components in the samples, which positively controls the  $G(t)$ . It can be said that a high  $K$  shows the hard deformation of viscous components, which lengthens the relaxation time. On the other hand, a small  $K$  demonstrates the large deformation of the viscous part during loading, reducing the  $G(t)$ . These results show the direct roles of yield stress and  $K$  in  $G(t)$ , confirming the established model.

Figure 7 exhibits the disparities of  $G(t)$  at unlike ranges of  $a$  and  $n$  using the advanced model.  $a = 0.2$  and  $n = 0.2$  maximize the  $G(t)$  to 5500 Pa, whereas the  $G(t)$  diminishes to 1400 Pa at  $a < 0.08$ . Accordingly, the high values of  $a$  and  $n$  parameters desirably support the  $G(t)$ , but only a low magnitude of  $a$  is enough to deteriorate the  $G(t)$ . These results

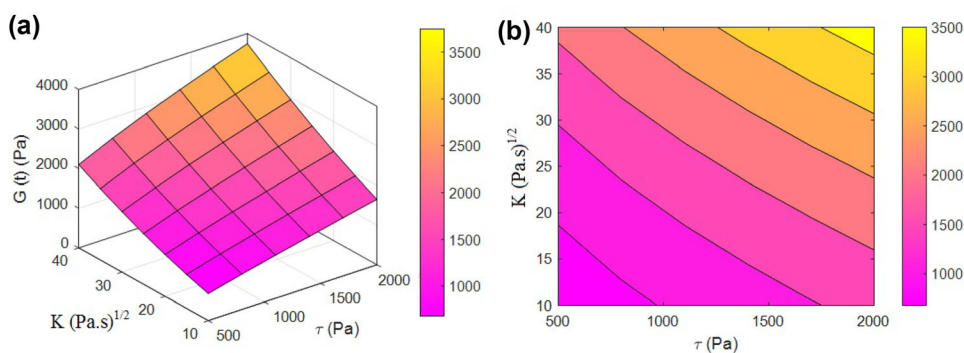


Fig. 6. Forecasts of  $G(t)$  at different values of yield stress and  $K$  according to Eq. (9): (a) 3D and (b) contour plans.

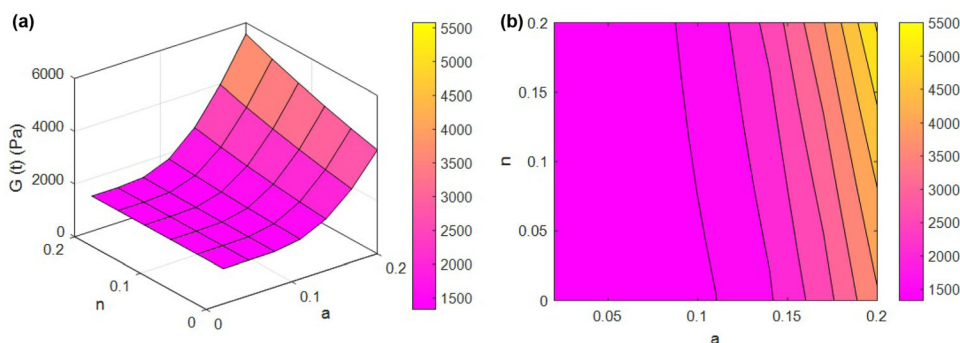


Fig. 7. Correlation of  $G(t)$  to  $a$  and  $n$  factors by the advanced model: (a) 3D and (b) contour plots.

demonstrate the vital character of  $a$  in the reduction of  $G(t)$ .

The wide Newtonian–power-law transition section delays the decrement of complex viscosity during the shear thinning process. Therefore, a high level of  $a$  positively increases the complex viscosity, which increases the storage modulus [Eq. (4)] and the  $G(t)$  [Eq. (2)]. In fact, a big transition section desirably raises the complex viscosity, which restricts the polymer's relaxation and promotes  $G(t)$ . On the other hand, a low level of  $a$  creates a short transition part, which extremely diminishes the complex viscosity and negatively develops the relaxation of polymer chains. The dominant role of poor  $a$  in  $G(t)$  reveals the importance of a short transition region on  $G(t)$ . These explanations show that the developed model appropriately reveals the significance of  $a$  on  $G(t)$ .

A low extent of  $n$  as power-law index establishes a strong shear thinning performance, which diminishes the complex viscosity and the relaxation time. Actually, low  $n$  seriously reduces the complex viscosity and facilitates the polymer's relaxation.<sup>53,54</sup> Nevertheless, a high value of  $n$  confines the reduction of complex viscosity during the frequency sweep test, which strengthens the polymer chains against relaxation and deformation producing a high  $G(t)$ . As a result, the  $n$  factor directly handles the  $G(t)$  in polymer systems, as expressed by the developed model.

## CONCLUSION

A reliable model for  $G(t)$  was established by various viscoelastic parameters using known models for storage and loss moduli. The model's results were matched to the experimental results of PLA/PEO and PLA/PEO/CNT systems. Furthermore, the parametric examinations of  $G(t)$  were expressed to legalize the advanced model. The forecasts successfully agreed with the experimental data. The blends demonstrate poor yield stress, but the attachment of CNT in nanocomposites results in a large yield stress. Also, CNT addition increases the relaxation time and zero complex viscosity, whereas the power-law index and transition width decrease in nanocomposites signifying that the nanoparticles deepen the shear thinning of polymers. Furthermore, the parametric analyses demonstrate that all parameters including zero complex viscosity, relaxation time,  $K$ , yield stress, power-law index and transition breadth directly affect  $G(t)$ . These reasonable impacts of whole factors on  $G(t)$  confirm the advanced model. This model suggests a simple methodology for calculating  $G(t)$  and viscoelastic terms in polymer blends and nanocomposites.

## CONFLICT OF INTEREST

The authors declare that they have no conflict of interest.

## REFERENCES

1. S. Liu, G. Wu, X. Chen, X. Zhang, J. Yu, M. Liu, Y. Zhang, and P. Wang, *Polymers* 11, 1015. (2019).
2. J. Shojaeiarani, M. Hosseini-Farid, and D. Bajwa, *Mech. Mater.* 135, 77. (2019).
3. O. Yousefzade, S. Valenti, J. Puiggali, H. Garmabi, and R. Macovez, *J. Polym. Sci. Part B Polym. Phys.* 57, 222. (2019).
4. R. Cui, K. Jiang, M. Yuan, J. Cao, L. Li, Z. Tang, and Y. Qin, *J. Market. Res.* 9, 10130. (2020).
5. M. Arastouei, M. Khodaei, S.M. Atyabi, and M.J. Nodoushan, *J. Market. Res.* 9, 14540. (2020).
6. S. Kim, Y. Zare, H. Garmabi, and K.Y. Rhee, *Sens. Actuators A* 274, 28. (2018).
7. Y. Zare, and K.Y. Rhee, *Compos. B Eng.* 158, 162. (2019).
8. Y. Zare, and K.Y. Rhee, *Polym. Compos.* 40, 4135. (2019).
9. C. Nakafuku, and M. Sakoda, *Polym. J.* 25, 909. (1993).
10. F. Carrasco, J. Gámez-Pérez, O. Santana, and M.L. MasPOCH, *Chem. Eng. J.* 178, 451. (2011).
11. M.A. Morsi, and M.H. Abd Elhamid, *J. Mater. Res. Technol.* 8, 2098. (2019).
12. M. Eryildiz, and M. Altan, *Polym. Compos.* 41, 757. (2020).
13. A.K. Mohapatra, S. Mohanty, and S. Nayak, *Polym. Compos.* 33, 2095. (2012).
14. S. Lebedev, O. Gefle, E. Amitov, D.Y. Berchuk, and D. Zhuravlev, *Polym. Test.* 58, 241. (2017).
15. Y. Zare, and K.Y. Rhee, *JOM* 72, 4323. (2020).
16. Y. Zare, and K.Y. Rhee, *JOM* 71, 3980. (2019).
17. V. Kumar, G. Lee, J. Choi, and D.-J. Lee, *Polymer* 190, 122221. (2020).
18. C. Mahmoudi, E. Demirel, and Y. Chen, *J. Appl. Polym. Sci.* 137, 49397. (2020).
19. M. Toozandehjani, K.A. Matori, F. Ostovan, K.R. Jamaludin, A. Amrin, and E. Shafei, *JOM* 72, 2283. (2020).
20. M. Soltanloo, M. Kazazi, S.E.H. Yeganeh, M.D. Chermahini, and B. Mazinani, *JOM* 72, 2235. (2020).
21. A. Adegbenjo, P. Olubambi, J. Westraadt, M. Lesufi, and M. Mphahlele, *JOM* 71, 2262. (2019).
22. A.M. Okoro, S.S. Lephuthing, S.R. Oke, O.E. Falodun, M.A. Awotunde, and P.A. Olubambi, *JOM* 71, 567. (2019).
23. R. Razavi, Y. Zare, and K.Y. Rhee, *Coll. Surf. A* 538, 148. (2018).
24. Y. Zare, and K.Y. Rhee, *J. Coll. Interface Sci.* 506, 283. (2017).
25. Y. Zare, K.Y. Rhee, and S.-J. Park, *Res. Phys.* 14, 102406. (2019).
26. Y. Zare, and K.Y. Rhee, *Eur. Polym. J.* 87, 389. (2017).
27. F. Hemmati, H. Garmabi, and H. Modarress, *Polymer* 55, 6623. (2014).
28. F. Hemmati, H. Garmabi, and H. Modarress, *Express Polym Lett* 7, 996. (2013).
29. M. Mohamadi, H. Garmabi, and M. Papila, *Polym. Bull.* 74, 2117. (2017).
30. B. Wang, T. Wan, and W. Zeng, *J. Appl. Polym. Sci.* 121, 1032. (2011).
31. F. Hemmati, and H. Garmabi, *Polym. Test.* 65, 78. (2018).
32. Y. Phua, W. Chow, and Z. Mohd Ishak, *Express Polym. Lett.* 5, 93. (2011).
33. A. Durmus, A. Kasgoz, and C.W. Macosko, *Polymer* 48, 4492. (2007).
34. M. Bousmina, and R. Muller, *J. Rheol.* 37, 663. (1993).
35. H.A. Barnes, J.F. Hutton, and K. Walters, *An Introduction to Rheology* (Elsevier, Amsterdam, 1989).
36. K. Yasuda, *Investigation of the Analogies Between Viscoelastic and Linear Viscoelastic Properties of Polystyrene Fluids* (Massachusetts Institute of Technology, Cambridge, 1979).
37. H. A. Barnes, *A Handbook of Elementary Rheology* (2000).
38. J. Domínguez, M. Oliet, M. Alonso, E. Rojo, and F. Rodríguez, *Ind. Crops Prod.* 42, 308. (2013).
39. J. Khademzadeh Yeganeh, F. Goharpey, and R. Foudazi, *Macromolecules* 43, 8670. (2010).
40. M. Tayefi, M. Razavi-Nouri, and A. Sabet, *Appl. Clay Sci.* 135, 206. (2017).



41. F. Schwarzl, *Rheol. Acta* 14, 581. (1975).
42. K.-W. Song, Y.-S. Kim, and G.-S. Chang, *Fibers Polym.* 7, 129. (2006).
43. W.-S. Bae, O.J. Kwon, B.C. Kim, and D.W. Chae, *Korea-Australia Rheol. J.* 24, 221. (2012).
44. E.C. Bingham, *Fluidity and Plasticity* (McGraw-Hill, New York, 1922).
45. D. Vlasveld, M. De Jong, H. Bersee, A. Gotsis, and S. Picken, *Polymer* 46, 10279. (2005).
46. Y. Zare, *Polymer* 72, 93. (2015).
47. Y. Zare, and H. Garmabi, *Appl. Surf. Sci.* 321, 219. (2014).
48. Y. Zare, A. Daraei, M. Vatani, and P. Aghasafari, *Comput. Mater. Sci.* 81, 612. (2014).
49. Y. Zare, K.Y. Rhee, and S.J. Park, *Res. Phys.* 15, 102562. (2019).
50. Y. Zare, K.Y. Rhee, and S.J. Park, *J. Biomed. Mater. Res. Part A* 107, 2706. (2019).
51. A. Rostami, H. Nazockdast, and M. Karimi, *RSC Adv.* 6, 49747. (2016).
52. A. Rostami, M. Masoomi, M.J. Fayazi, and M. Vahdati, *RSC Adv.* 5, 32880. (2015).
53. A. Poslinski, M. Ryan, R. Gupta, S. Seshadri, and F. Frechette, *J. Rheol.* 32, 703. (1988).
54. S. Theron, E. Zussman, and A. Yarin, *Polymer* 45, 2017. (2004).

**Publisher's Note** Springer Nature remains neutral with regard to jurisdictional claims in published maps and institutional affiliations.